# Atomic layer deposition of palladium coated TiO2/Si nanopillars: ToF-SIMS, AES and XPS characterization study

Igor Iatsunskyi, Gloria Gottardi, Victor Micheli, Roberto Canteri, Emerson Coy, Mikhael Bechelany

# Atomic Layer Deposition of Palladium Coated $TiO_2$/Si nanopillars: ToF-SIMS, AES and XPS characterization study

Igor Iatsunkyi[1*], Gloria Gottardi[2], Victor Micheli[2], Roberto Canteri[2], Emerson Coy[1], Mikhael Bechelany[3]

1. *NanoBioMedical Centre, Adam Mickiewicz University, Wszechnicy Piastowskiej 3, 61-614, Poznan, Poland*
2. *Fondazione Bruno Kessler, Center for Materials and Microsystems, Via Sommarive 18, 38123 Trento, Italy*
3. *Institut Européen des Membranes, IEM, UMR 5635, Univ Montpellier, ENSCM, CNRS, Montpellier, France*

Corresponding authors*: yatsunskiy@gmail.com, igoyat@amu.edu.pl

**Key Words:** Silicon nanopillars; $TiO_2$; Pd; Atomic Layer Deposition; Time-of-Flight Secondary Ion Mass spectrometry; X-Ray photoelectron spectroscopy; Auger spectroscopy.

## Abstract

Nanocomposite based on Palladium (Pd) Coated $TiO_2$/Si nanopillars is an attractive candidate for photocatalytic applications because of its outstanding electrochemical and optical characteristics. In this research, Pd/$TiO_2$/Si nanopillars were synthesized by combination of metal-assisted chemical etching and atomic layer deposition, and then the surface was investigated by means of Electron microscopy, Time-of-Flight Secondary Ion Mass-Spectrometry (ToF-SIMS), Auger Electron Spectroscopy (AES) and X-Ray Photoelectron spectroscopy (XPS). The spatial distribution of different chemical components and contaminations on the surface of the produced nanocomposites was evaluated by ToF-SIMS mapping. Depth profiling by AES was carried out to determine the chemical composition and the conformality of Pd and $TiO_2$ layer over the Si pillars. The elemental composition and stoichiometry were determined by XPS analysis. The XPS valence band analysis was performed in order to investigate the modification of $TiO_2$/Si nanopillars electronic structure after Pd deposition. It was found that the Pd coating decreases the concentration of photoactive defects that can reduce the photoelectrochemical efficiency of $TiO_2$.

## 1. Introduction

One dimensional (1D) core-shell nanocomposites based on silicon, metal oxide (MOx) and noble metals have drawn increased attention in different applications, such as in surface wettability [1], (bio)sensors [2,3], energy [4], and (photo)catalysis [5]. It was shown that silicon nanopillars (SiNP) covered by metal oxides (e.g. ZnO, $TiO_2$) demonstrate an enhanced efficiency towards oxygen evolution reaction (OER) and may be applied as an effective photoanodes for solar water splitting processes [5,6]. Metal oxide coatings (shell structure) of 1D Si (core) nanostructures play a significant role in the photocatalytic processes [7]. The heterojunction of MOx-Si affects the recombination rate and the absorbance properties, and as a consequence, enhance the photoelectrochemical (PEC) performance of MOx/SiNP nanocomposites [8,9]. Recently, it was also demonstrated that the photoactive nanoparticles based on junctions of noble metals and MOx may enhance carrier transport capabilities of photogenerated carriers thus providing a more efficient photocatalytic water splitting [10,11]. However, the conformal Pd coating slightly diminishes the photoactivity towards OER of the nanostructures due to the Schottky contacts generated by the Pd-$TiO_2$ nanojunctions [12]. On the other hand, the Pd layer in Pd/$TiO_2$/SiNP nanocomposites boosts the hydrogen evolution reaction (HER), still remaining competitive for the biased OER. Therefore, the combination of three components (SiNP, $TiO_2$ and Pd) makes these nanocomposites highly applicable in photo- and electro- catalytic performance.

In order to produce robust and highly stable photoelectrodes based on metal/MOx/SiNP nanostructures, it is important to study not only the structural, mechanical, chemical, electronic and PEC properties, but to find factors which may reduce their stability and efficiency. Among these factors, one may include surface contaminations, inhomogeneous material distributions and finally bulk and interface defects. Wherever surface or thin film composition plays a critical role in performance, it is crucial obtaining a thorough characterization using some extremely surface sensitive techniques, which could provide complementary analysis of the nanocomposite. Electron and mass spectroscopy techniques are considered to be the most effective experimental methods to study the elemental composition and electronic properties of the surface and near-surface area of materials [13,14]. For instance, X-Ray photoelectron (XPS) and Auger electron spectroscopy (AES) enable to determine the surface chemical composition, the phase, the stoichiometry, the valence band (VB) structure, the type and concentration of defects [15–17] with a maximum sampling depth of 10 nm, which can be increased if the analysis is performed after eroding the surface with an ion gun (depth profiling). On the other hand, time of flight secondary ion mass spectrometry (ToF-SIMS), being an even more surface sensitive technique (1-2 monolayer), is particularly suitable to detect organic and inorganic surface contaminations of the

studied nanocomposites [18,19]. These experimental approaches give the full analysis of the nanocomposites and may reveal both positive and negative factors of produced photoelectrodes.
Here we report a detailed study of the chemical composition and electronic properties of 1D core-shell Pd/$TiO_2$/SiNP nanocomposites. SiNP, as a core, were obtained by metal-assisted chemical etching (MACE) and nanosphere polymer lithography (NPL). The highly uniform and conformal shell layer consisting of Pd and $TiO_2$ was produced by atomic layer deposition (ALD) method. The structure and the surface morphology of Pd/$TiO_2$/SiNP nanocomposites were studied by scanning electron microscopy (SEM), and transmission electron microscopy (TEM) with an EDX analyzer. The chemical analysis and electronic properties of produced nanocomposites were investigated by XPS, AES and Tof-SIMS. In this study, we also concentrated on the analysis and evaluation of defects in the $TiO_2$ layer. A possible mechanism of photocatalytic behavior changes after the Pd deposition was proposed. The experimental results and conclusions obtained and presented in this work may improve the PEC water splitting performance and other (photo)catalytic applications of Pd/$TiO_2$/SiNP nanocomposites where it is important to tune and control chemical and electronic properties of photoelectrodes.

## 2. Experimental

### *2.1.Pd coated $TiO_2$/Si nanopillars fabrication*

In order to produce SiNP we used a method based on the combination of nanosphere lithography (NPL), reactive ion etching (RIE) and metal-assisted chemical etching (MACE) described elsewhere [5,7]. Briefly, the low-resistive (0.01-0.02 ohm•cm) n-type silicon samples (1x1 $cm^2$) were cleaned by ethanol, acetone, and dionized water (DI). Then, polystyrene nanospheres (mean diameter 800 nm) were deposited on a Si surface by spin-coating technique and etched by oxygen plasma to reduce the size of the nanosphere using a RIE process (MicroSys 200; RF power – 70 W, pressure – 0.6 mbar). After that, a 50 nm thick layer of gold was deposited by magnetron sputtering machine (Quorum Q160T). MACE was performed in the etchant solution containing hydrofluoric acid (HF, 40%), Hydrogen peroxide ($H_2O_2$, 30%), and ultrapure $H_2O$ at a ratio of 80:80:20, respectively. After removing of the Au layer using a solution of Aqua Regia (hydrochloric acid(HCl, 35%) and nitric acid ($HNO_3$, 65%) at ratio 1:2), samples of SiNP were cleaned and dried. In order to deposit $TiO_2$ over the SiNP, ALD technique was applied. The ALD $TiO_2$ layer was deposited using titanium chloride ($TiCl_4$) (0.5 s exposure) and water (0.5 s exposure) as precursors at 200 °C. We applied 400 ALD cycles which corresponds to a 18-20 nm thick layer of $TiO_2$ on the planar Si surface (the growth rate is around 0.45 Å/cycle). The Pd coating was achieved by applying 200 ALD cycles at 220 °C using $Pd(hfac)_2$ (15 s exposure) and formalin

(15 s exposure) as precursors. In palladium ALD growth studies using $Pd(hfac)_2$, various reducing agents were utilized such as hydrogen, hydrogen plasma, glyoxiclic acid and formalin. Among them formalin is the most used one due to easy handling. In fact, the commonly used formalin coreactant can effectively removes the precursor hfac ligands and reduces the Pd (II) to Pd (0) state, leaving single Pd atoms at the substrate surface [20]. The typical ALD process of Pd deposition is described previously [12]. After all procedures, we obtained three sets of samples: (i) SiNP, (ii) $TiO_2$/SiNP and (iii) Pd/$TiO_2$/SiNP samples [12].

*2.2.Characterization*

Structural properties and morphology were studied by Scanning Electron Microscopy (SEM) (JEOL JSMM7001F) and High-Resolution Electron Microscopy (HR-TEM) (JEOL ARM 200F). Electron microscopes were equipped with an Energy Dispersive X-ray Spectroscopy (EDX).

The TOF-SIMS system used in this study was a mass spectrometer from ION TOF (TOF- SIMS IV) equipped with an analysis gun with Bismuth (Bi) source operating at 25KV of energy. The cluster ion $^{209}Bi_3^+$ was rastered over an area of 500x500μm$^2$. The pulse length was 30ns and the total ion dose was kept below the static regime of $10^{12}$ ions/cm$^2$. High mass resolution spectra were acquired in the bunched mode (m/Δm ~5000) at a spatial resolution of about 6-10μm.

Auger measurements were performed in a PHI model 4200 Thin Film Analyzer, equipped with a variable resolution Cylindrical Mirror Analyzer (CMA) and a coaxial electron gun. The system base pressure was $2.0x10^{-9}$ Torr. Depth profiles were obtained by alternating sputtering and acquisition cycles. A 2KeV Ar beam, rastered over an area of 2 mm, sputtered the samples, while a 2 KeV, 200 nA electron beam excited the Auger electron. The analyzed area was 400 μm$^2$. Electron gun and ion gun parameters have been set in order to achieve appropriate and suitable analytical conditions for effectively analyzing the samples both on the surface and throughout the full coating with good depth resolution.

XPS (X-ray Photoelectron Spectroscopy) spectra were recorded with a KRATOS Axis DLD Ultra instrument (Kratos – Manchester, UK) equipped with a hemispherical analyzer and a monochromatic Al Kα (1486.6eV) X-ray source. The broad spectra (survey) were acquired at 160 eV pass energy, while a higher resolution was used for the acquisition of the core lines, which was performed setting the pass energy at 20 eV. This allowed to reach an energy resolution of ~0.4 eV. The analyses were performed at 90° of tilt of the sample with respect to the analyzer. The spectra were fitted using a homemade software (R-XPS) based on R-platform [21]. After a Shirley-type background subtraction, Gaussian-Lorentzian peak shape was used for the single core lines deconvolution. Since the deposited films were exposed to air, the C1s peak must include a significant amount of spurious carbon due to ambient contamination. After deconvolution of the

C1s core line therefore, the main peak at 285 eV corresponding to hydrocarbon contamination was used as internal reference to calibrate the spectra. For the quantification of the different components, experimental sensitivity factors (RSF) were used. Quantification accuracy (in terms of relative atomic concentration) has been evaluated in the order of 0.5-1%.

## 3. Results and Discussion

### *3.1. Morphology of Pd/$TiO_2$/SiNP*

In our previous researches, it was shown that the photocatalytic efficiency of nanocomposites based on Pd/$TiO_2$/SiNP, ZnO/$TiO_2$/SiNP and $TiO_2$/SiNP depends not only on the composition of produced photoelectrodes but also on their structure and morphology [5,6,12]. The structural properties and morphology of the produced Pd/$TiO_2$/SiNP samples were studied by electron microscopies combined with an EDX analysis and some results are presented in Figure1. Panel (a) shows the surface of the sample after the MACE procedure. It is visible how the pillars are distributed in a hexagonal manner covering the whole surface of the Si. Depending on the parameters of NPL and MACE, we could produce pillars with different morphology. The cross-sectional TEM image of the Pd/$TiO_2$/SiNP is displayed in panel (b). We estimated an average diameter of pillars around 650 ± 50 nm, average length 3.0 ± 0.2 μm, with a period of 400 ± 50 nm. Figure 1b shows finally with higher magnification the walls of the pillars and their EDX cross-sectional mapping. The image allows to visualize the core-shell structure of the produced Pd/$TiO_2$/SiNP, where the Pd coating is a shell, Si is the core and $TiO_2$ partly penetrates inside the porous matrix of initial pillars and it also covers SiNP creating sublayer between Pd and Si. It was shown that the $TiO_2$ sublayer in the Pd/$TiO_2$/Si heterojunction increases the charge carrier separation and enhances photocatalytic efficiency [12].

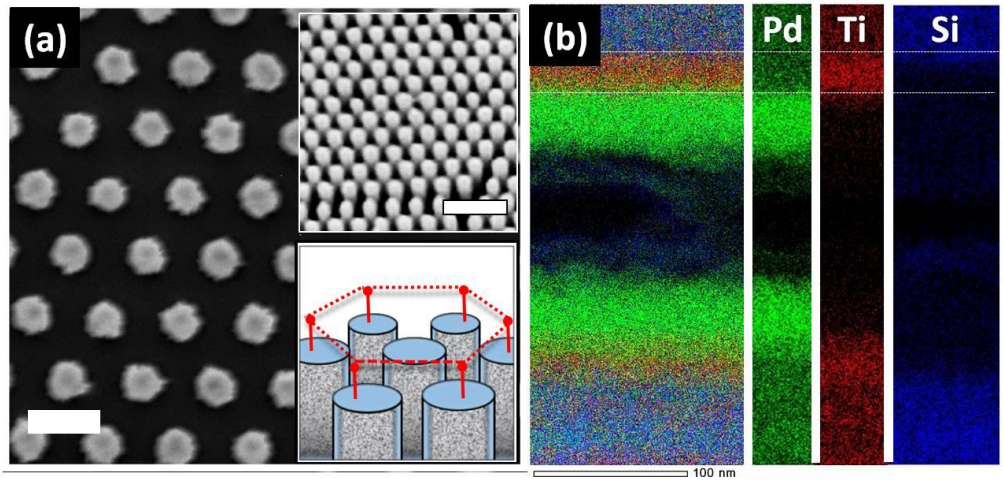


**Figure 1**. (a) SEM images (scale bar – 1um), and (b) cross-sectional TEM/EDX mapping of Pd/$TiO_2$/SiNP

### *3.2. TOF-SIMS analysis*

ToF-SIMS is considered to be a very useful and surface sensitive (1-2 monolayers of sampling depth) technique in the study of the surface properties and composition of nanomaterials. The positive mass spectra for all spectra is presented in the Figure S1 (Supporting information). The most intense SIMS signals of SiNP are attributed to $Si^+$ and to some hydrocarbon contaminations (e.g. $C_2H_3^+$, $SiC_3H_9^+$). After deposition of $TiO_2$, one may observe also peaks associated with titanium ions ($Ti^+$, $TiO^+$, $TiO_2H^+$, $Ti_3O_5^+$) and again hydrocarbon contaminations ($C_2H_3^+$, $C_3H_3O^+$) which probably remain from the SiNP sample. ToF-SIMS analysis of the Pd/$TiO_2$/SiNP sample showed on the other hand the presence of palladium ions. Mostly, it was non-oxidized form of palladium ($Pd^+$, $Pd_2^+$). However, a small amount of the oxidized Pd ($Pd_2O^+$) was also detected.

The ToF-SIMS mapping enables to evaluate the spatial distribution of different chemical components on the surface of the produced nanocomposites. The ToF-SIMS maps for SiNP, $TiO_2$/SiNP and Pd/$TiO_2$/SiNP samples are presented in Figure 2. They show the differences in the intensity of the signals corresponding to the presence of $Si^+$, $Ti^+$, $Pd^+$ and some carbon contaminations. It was shown in particular that surfaces of SiNP, $TiO_2$/SiNP and Pd/$TiO_2$/SiNP samples are contaminated by PDMS (Poly-dimethyl siloxane).

It is worth noting that the ToF-SIMS mapping demonstrated the inhomogeneous distribution of metal elements (see $Ti^+$, $Pd^+$). It is also visible an increased concentration of $Ti^+$ and $Pd^+$ in the area with a high SIMS signal from hydrocarbon contaminations. The inhomogeneous distribution of active catalytic materials causes a non-uniformity of the electrical potential over the surface, and as a consequence, it modifies the (photo)catalytic activity of the produced photoelectrodes. Therefore, it is extremely important to eliminate all polymer contaminations from Si substrate (in this case SiNP) before ALD processes. SEM analysis proved that some polymer residuals remain even after the thorough chemical cleaning of SiNP surfaces (SI, Figure S2). The oxygen plasma cleaning allowed eliminating completely polymer contaminations from the SiNP. It means that this type of surface cleaning should be applied before ALD processes.

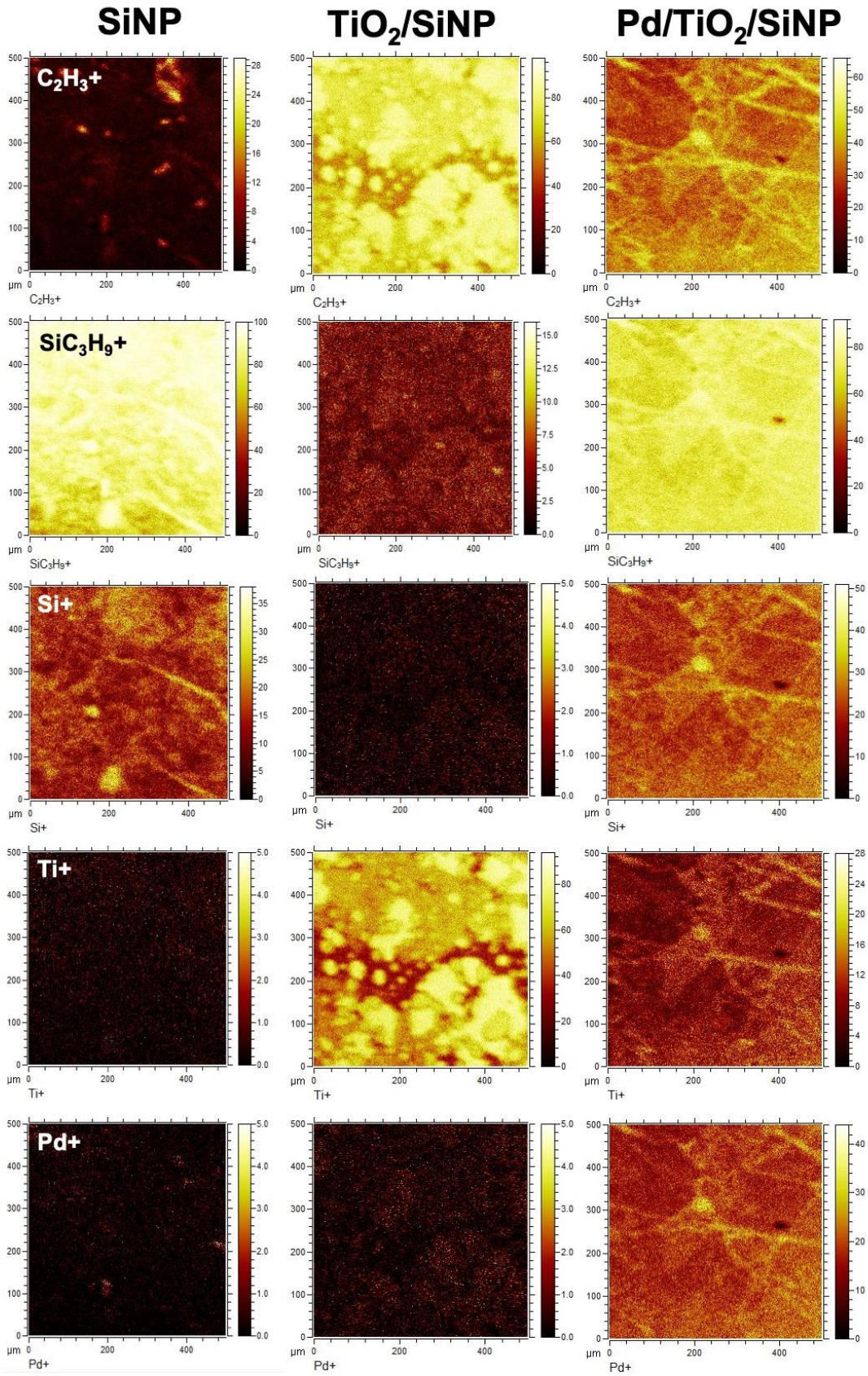


**Figure 2**. Tof SIMS ion maps (lateral distribution of some elements) for SiNP, $TiO_2$/SiNP and Pd/$TiO_2$/SiNP samples.

*3.3. Auger Electron Spectroscopy studies*

AES surface analysis and depth profiling were used to investigate the surface and the bulk chemical composition of the produced samples. Five survey spectra were acquired on the surface of each sample. A 400 $um^2$ area of analysis was arbitrarily chosen on the surface of the sample. Figures 3S, 4S and 5S (Supporting Information) show the Auger spectra acquired on the surface of SiNP, $TiO_2$/SiNP and Pd/$TiO_2$/SiNP samples. The measured derivative intensities of $C_{KLL}$ (272 eV), $O_{KLL}$ (503 eV), Si $_{LVV}$ (76 eV oxidized and 92 eV elemental), Ti $_{LMM}$ (387 eV), $Cl_{LMM}$ (181 eV), $S_{LMM}$ (152 eV), and $Pd_{MNN}$ (330 eV) Auger transitions have been used to determine the relative atomic concentration of the different elements for each individual spectrum. Specifically, Auger quantification has been achieved by applying an elemental relative sensitivity factors (SF's) method to the peak height data.

It is worth to be noted here that the LVV transition of silicon (as for several metals) involves valence electrons which, being sensitive to chemical environment (chemical state) influence both the position or/and the shape of the Auger peak. Analysis of the peak shift is, namely, useful for identifying the different oxidation state of silicon and more particularly the $SiO_2$-76 eV transition is related to the maximum oxidized state of silicon ($SiO_2$) whereas the Si-92 eV peak is associated to the elemental silicon. In this sense, Table 1 provides an overview of the average surface concentration data for each sample.

**Table 1**. Sample Average Surface Relative Atomic Concentration (%)

| Element / Sample | C | Ti | O | Si | Pd | Cl | S |
|---|---|---|---|---|---|---|---|
| **SiNP** | 25.2±1.4 | | 42.8 ±1.8 | 30.9 ± 0.4 | | 0.6 ± 0.2 | 0.5 ± 0.5 |
| **$TiO_2$/SiNP** | 14.7±1.1 | 32.6±1.0 | 52.2 ±0.7 | | | 0.3 ± 0.1 | 0.2 ± 0.2 |
| **Pd/$TiO_2$/SiNP** | 17.7±3.5 | 17.8±1.4 | 32.9±1.8 | 14.1±1.6 | 11.1±0.5 | 1.1±0.5 | 5.9±0.5 |

From data in Table 1, it is clearly visible that SiNP sample surface is mainly characterized by three elements (Si, O and C). Carbon signal is associated with hydrocarbon contaminations remained after MACE. The high concentration of oxygen (>40%) but mostly the kinetic energy shift of $Si_{LVV}$ transition, that is typical for oxidized silicon, indicate on the other hand, that surface silicon is present as sub-stoichiometric oxidized silicon ($SiO_x$). The deposition of $TiO_2$ by ALD onto SiNP samples is evidenced by an increasing of oxygen concentration up to 52 at% and the appearance of Ti signal (32 at%). Interestingly, there are no peaks associated with Si, which means the fully coverage of pillars by $TiO_2$ layer was achieved. Detected chloride and sulfur surface contaminations for SiNP and $TiO_2$/SiNP samples were less than 1%.

Finally, AES surface analysis of the Pd/$TiO_2$/SiNP sample shows the presence of Pd (11.1 at%), C (17.7 at%), O (32.9 at%), Ti (17.8 at%), and again Si (14.1 at%). One may assume that during palladium deposition some restructuration of the $TiO_2$ layer occurs, thus disrupting the continuity of the film. We have to consider, in fact, that in order to deposit a Pd layer, two ALD precursors ($Pd(hfac)_2$ and formalin) have been used at 220° C. Probably, fluoride residuals present in the reaction chamber may have etched the $TiO_2$ layer. However, this assumption needs to be investigated thoroughly in further research.

Figure 3 shows the AES depth profiles acquired on the SiNP, $TiO_2$/SiNP and Pd/$TiO_2$/SiNP samples. Combining the AES measurements with argon bombardment, the surface layer can be gradually removed and the analysis can be carried out on the new layers exposed after each sputtering cycle. This is known as depth profiling and it provides the relative atomic concentrations of the various elements as a function of the depth. An average erosion rate (i.e. sputtering rate) of 1.56 nm/min was calculated on a 100 nm $SiO_2$/Si reference film. This value was then applied to determine the erosion time into erosion depth conversion for all depth profiles.

The depth profile of the as received SiNP sample (Figure 3a) shows a distribution of silicon, oxygen and carbon that changes when considering the outer 30 nm thin region and the bulk region, respectively. The superficial region, namely that of the superficial silicon oxide, is characterized by a rather rapid decrease of oxygen, carbon and oxidized silicon which corresponds to an equally rapid increase of elemental silicon. Penetrating more in depth, all signals exhibit the same but slower trend. It is worth to remark that oxygen and oxidized silicon signals are detected throughout the whole analyzed volume of the sample, although their concentration decreases with depth. C is also observed as contaminant both on the surface and in the investigated volume. The presence of these elements into the bulk region may be explained by the nanopillars nature of the sample. The depth profile of the $TiO_2$/SiNP sample is shown in figure 3b. A well-defined titanium oxide surface layer can be observed. Except for the near-surface region (0÷5 nm) where some carbon was detected, no contamination is present into the $TiO_2$ layer. A quite large interface with silicon substrate can be observed in this profile. Elemental silicon and oxidized silicon increase while titanium/oxygen decrease until a steady distribution plateau was reached (Ti≈31%, O≈35%, $Si_{EL}$≈26%).

Finally, Figure 3c displays the in-depth analysis of the Pd/$TiO_2$/SiNP sample. A relatively distinct layer of titanium oxide can be identified. However, in the most superficial layers titanium distribution exhibits a not negligible depletion corresponding to the presence of palladium nanoparticles. Once the depth profile analysis penetrates the near surface region in fact, Pd concentration increases rapidly to around 12% (revealed at 1 nm depth) and then decreases with erosion depth. The depth profile is actually not showing a clean palladium thin layer but rather a

Pd-Ti co-presence region. Correspondingly, Ti and O signals increase until the profile reaches the interface with silicon and then they decrease. Small amount of carbon (≈4%) and oxidized silicon (≈2%) was detected in this region while no evidence of elemental silicon was found. AES depth profiling enables to estimate the thickness of the Pd layer which was around 20 nm and correlates well with TEM analysis. Besides, it is clearly highlighted that the ALD process allows Ti to penetrate inside SiNP. This phenomenon is related to both the porous structure of the produced pillars [7] and the highly conformal character of the deposition technique. $TiO_2$ nanocrystallites inclusions in the porous matrix not only improve the mechanical properties of SiNP but also enhance their photocatalytic efficiency due to the $TiO_2$-Si multi-junctions formation and, as a consequence, the fast photogenerated charge carrier separation.

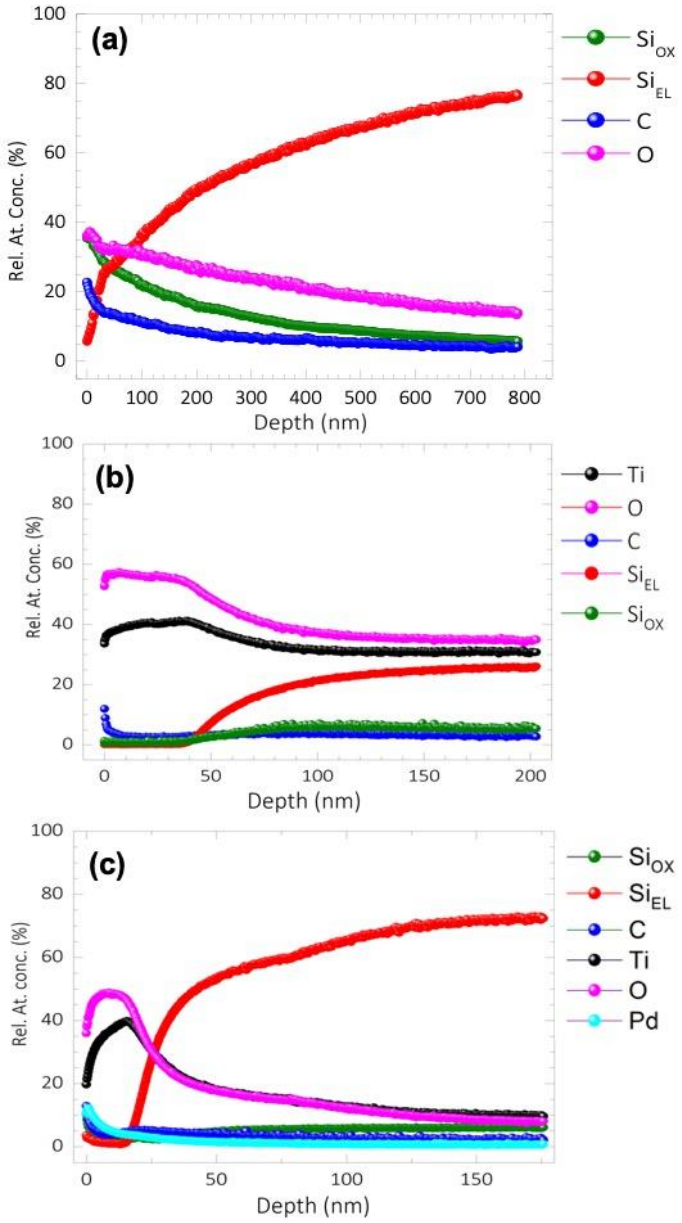


**Figure 3**. AES depth profile of (a) SiNP, (b) $TiO_2$/SiNP and (c) Pd/$TiO_2$/SiNP samples. The relative atomic concentration of elements is plotted as a function of depth (calculated from erosion time).

*3.4. X-ray photoelectron spectroscopy studies.*

*3.4.1. Survey spectra*

In the final stage, the XPS analysis was applied to study chemical composition and electronic properties of the produced nanocomposites. Figure 4 shows the survey spectra of the analyzed samples. Except an abundant contamination of carbon, the survey spectrum of SiNP is dominated by the signals of silicon and oxygen elements. The hydrocarbons contamination is highly present on the Si surface (around 30%-35% if we consider the oxidized components). It is also visible a small contamination of chlorine. The spectrum of the $TiO_2$/SiNP sample displays the signals of Ti, O and C. No signal from Si is clearly visible from the survey in this case. Its presence has been checked by acquiring a detailed spectrum in the region of Si 2p core line, in order to verify if a small signal coming from the substrate surface oxide is still visible (shown later). Small contaminations of N and Cl atoms are present, but at the limit of the instrument sensitivity. The survey of Pd/$TiO_2$/SiNP sample demonstrates the deposition of Pd on the $TiO_2$/SiNP surface. The spectrum is dominated by the signals of Ti, Pd, O and C. The signal coming from the Si substrate is also visible from the survey of the Pd/$TiO_2$/SiNP sample.

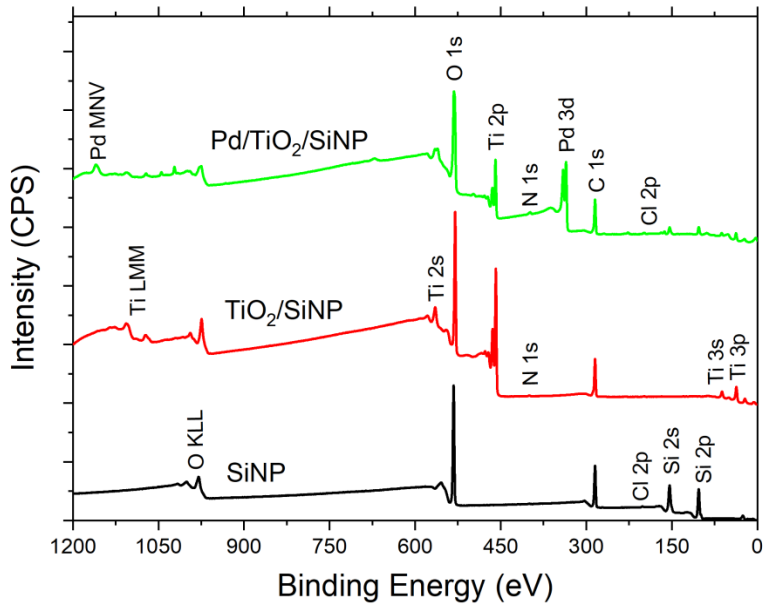


**Figure 4**. XPS survey spectra of the SiNP (black curve), $TiO_2$/SiNP (red curve) and Pd/$TiO_2$/SiNP (green curve). The main core levels are labeled. The data are normalized to each O1s peak maximum and separated vertically.

The modified Auger parameter analysis is one of the useful methods to determine the phase and chemical state in XPS, because it uses the difference between the photoelectron peak and the Auger

peak and it needs no correction of the peak position even if peak shift due to the charging. [22] The modified Auger parameter ($E_K^{Auger\ peak}$ +$E_{BE}$) was calculated, what allowed us to define the stoichiometry, the phase and the crystallinity [22]. Calculations lead to a value of 1042.1 eV and 662.7 eV for $TiO_2$/SiNP and Pd/$TiO_2$/SiNP samples, corresponding to the stoichiometric $TiO_2$ and the metallic Pd, respectively [22,23].

*3.4.2. XPS core-level spectra of $TiO_2$/SiNP and Pd/$TiO_2$/SiNP samples*

The detailed XPS spectra of O1s and Si2p for SiNP sample and of O1s and Ti2p for the $TiO_2$/SiNP one are shown in the Figure 5. In addition, XPS core-level spectra for carbon components are presented in the SI (Fig. S6). Analyzing the O1s core line acquired on the SiNP surface, it was found that the peak could be deconvoluted into four components. Components #1 and #2 (around 532.5 eV and 531 eV) originate from the oxidized carbon contamination and the non-stoichiometric oxides formed by silicon ($Si_XO_y$) [15]. The silicon dioxide ($SiO_2$) finds its correspondent in the component #3 of O1s core line, which is mainly due to its contribution. A broadening of the O1s core line at high BE justify the presence of a fourth component, most probably due to the presence of adsorbed OH groups (water). In the Si core line (panel (b)), it is clearly visible the metallic component, with the spin-orbit doublet which can be easily resolved (components #1- 103 eV and #2 – 99 eV) [24]. The silicon oxide layer generates a broad peak at higher binding energies, which can be resolved by overlapping at least 3 components (#3-#5), due to the different possible oxidation states of Si.

Panels (c) and (d) of Figure 5 show the O1s and Ti2p core lines for the $TiO_2$/SiNP sample. After charging correction, the presence of an asymmetric shoulder at the higher binding energy side of O1s core line, indicates the existence of different chemical states of oxygen. The peak is deconvoluted into 4 components: the first one at lower binding energy (530.11eV) is the main component and can be ascribed to the O1s core peak due to $O^{2-}$ bound to $Ti^{4+}$ in $TiO_2$. The second component at higher BE, located at 531.23eV, may arise due to the oxygen contribution in Ti-OH bonds (Ti hydroxide species) and/or in $Ti_xO_y$ phase where Ti has a lower oxidation state ($3^+$, as in $Ti_2O_3$). The third and fourth components, at 532.09eV and 532.97eV, are associated to carbonaceous contaminations and adsorbed molecular water. The Ti 2p doublet was fitted with two main components located at 458.67 eV and 464.44 eV, corresponding to the Ti $2p_{3/2}$ and Ti $2p_{1/2}$ spin-orbit doublet, respectively. The BEs peak separation of 5.77 eV and the peak position confirms that the main oxidation state of Ti is $4^+$ [25]. The core line shows also an additional shoulder at lower binding energies, which was resolved adding two additional components at 457.12eV and 462.92eV, which indicate the presence of lower oxidation states ($Ti^{3+}$) for Ti. The appearance of lower oxidation states may be due to the formation of the $Ti_2O_3$ phase or to the

presence of oxygen vacancies, that is to say of defects in the $TiO_2$ crystal lattice. We calculated the oxygen to metal ratio in the oxide, which is a useful parameter to estimate the stoichiometry of the latter and the existence of defects (oxygen vacancies). To determine such parameter only the main component of oxygen (O 1s) which bounds to Ti in the $TiO_2$ lattice was used, while for the Ti, the whole area of the Ti 2p spectrum. In this way, we obtained the O/Ti ratio value of 1.87, which by being less than 2, justifies the supposition of defects in the oxide layer. It was shown in many researches that defects in $TiO_2$ enhance its photocatalytic efficiency [26,27]. Therefore, it is extremely important to consider defects, their concentration and type, while studying photoelectrochemical properties of nanocomposites based on $TiO_2$.

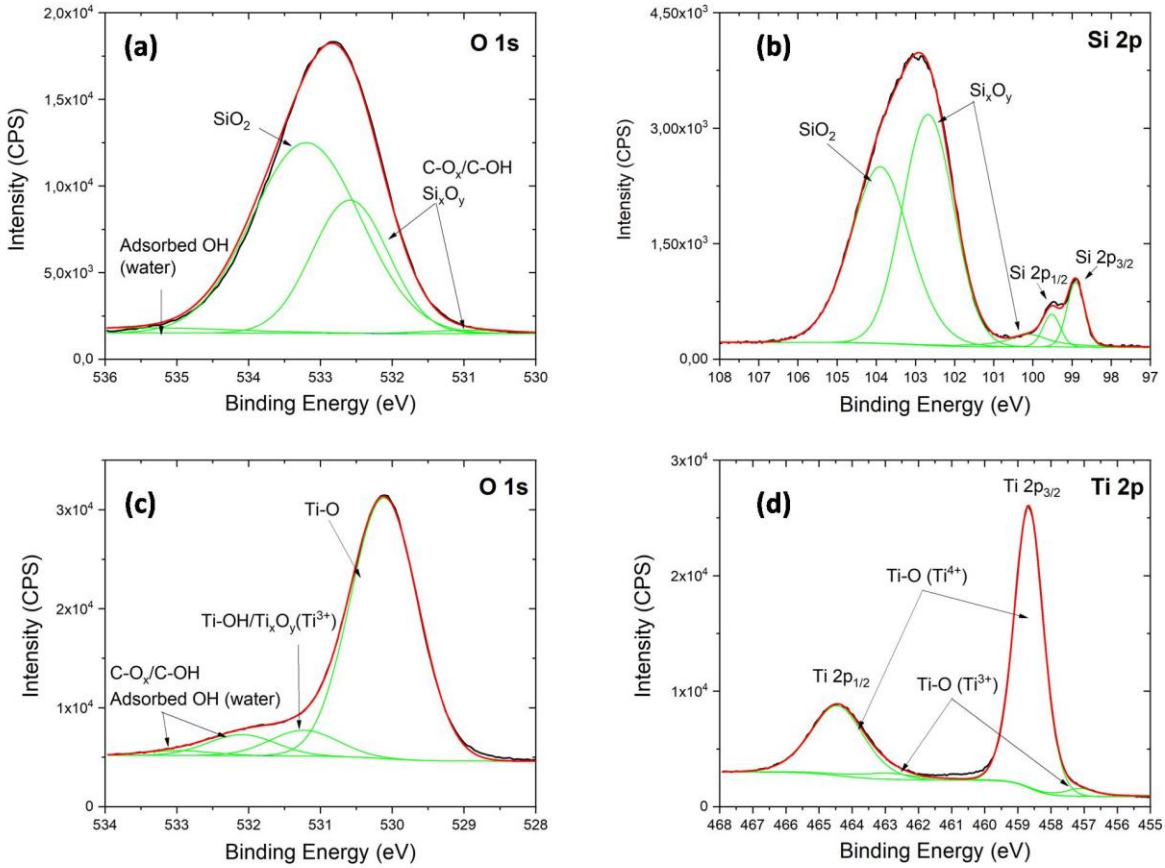


**Figure 5**. XPS core-level spectra of (a) O 1s, (b) Si 2p for SiNP, and (c) O 1s, Ti 2p for $TiO_2$/SiNP samples. In green, the deconvoluted components of XPS core-level spectra.

Figure 6 demonstrates core-level spectra for the Pd/$TiO_2$/SiNP sample. The O1s core line is rather complex in this sample, due to the different chemical states of oxygen bound to different metals (mainly Ti, but also Pd and Si) as well as the contribution of the Pd 3p core line, which overlaps with the O1s region. The O1s peak has been therefore deconvoluted into 6 components, but only the first 4 are attributed to oxygen. The last 2 ones generate from the Pd 3p signal and were not

considered, obviously, in the quantification. The first component of O 1s #1 at lower BE (528.9eV) is due to the bond Pd-O, while the second one at 530.5 eV to the titanium oxide ($O^{2-}$ bound to $Ti^{4+}$ in $TiO_2$ phase). The third component located at 531.3eV is much probably due to the oxygen contribution in metal hydroxide species (Ti-OH) [25]. The fourth component at 532.5eV is finally associated to carbonaceous contaminations, silicon oxide and adsorbed molecular water. The considerations made on O1s core line find confirmation in the detailed analyses of the Si 2p, Ti 2p and Pd 3d peaks. The Ti 2p doublet was fitted with two main components located at 459.29 eV and 465.00 eV, respectively. The BEs peak separation of 5.77eV and the peak position confirms that the main oxidation state of Ti is 4+ [25]. However, analyzing two additional components at 457.8eV and 463.5eV, which could indicate the presence of lower oxidation states or defects, the fit quantification gave very little values for these two components. Besides, the calculated value of the O/Ti ratio was 2, which indicates a good stoichiometry of the Ti oxide. It means that, after the ALD Pd deposition, the phase composition of the $TiO_2$ layer improves. Most probably the Pd ALD process leads to the decrease of defects concentration in $TiO_2$. One may assume that, during the Pd deposition, the defects present in the near-surface area of $TiO_2$ are passivated. This should lead to the decrease of photoelectrochemical properties of $TiO_2$.

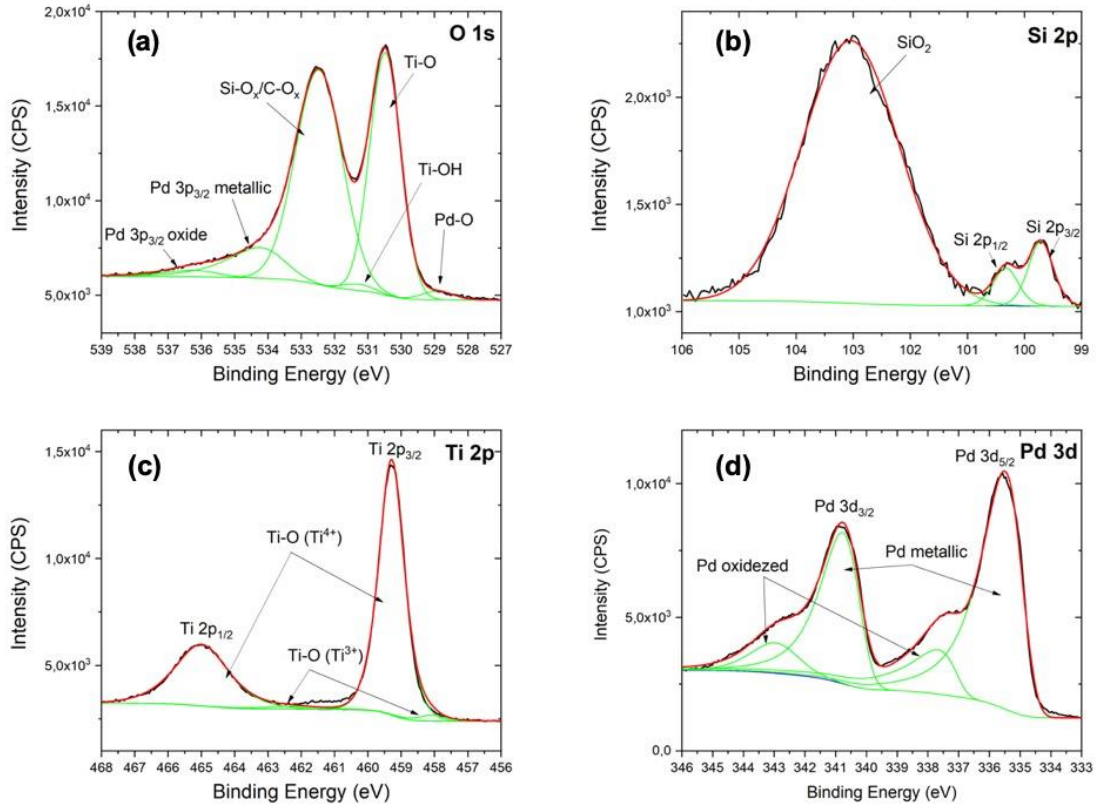


**Figure 6**. XPS core-level spectra of (a) O 1s, (b) Si 2p, (c) Ti 2p and (d) Pd 3d for the $Pd/TiO_2/SiNP$ sample. In green, the deconvoluted components of XPS core-level spectra.

As for the Pd 3d peak, it has been resolved with four components: one doublet due to the metallic part of palladium (#1 and #2 at 335.50eV and 340.78eV, corresponding to the non-oxidized spin orbit doublet Pd $3d_{5/2}$ and Pd $3d_{3/2}$); the second one, at higher BEs, due to the oxidized component, but it is actually very small with respect to the metallic one [23] (SI, Table S1). This confirms the predominantly metallic form of the deposited noble metal, with only a thin layer of oxide on the surface of the Pd nanoparticles.

### *3.4.3. Valence band analysis*

It is well known that the valence band (VB) analysis can provide valuable information about the existence of defects (e.g. oxygen vacancies) in metal oxides and allows to investigate the modification of nanocomposites electronic structure. To this purpose, we acquired the VB spectra for all samples, which are shown in figure 7a.

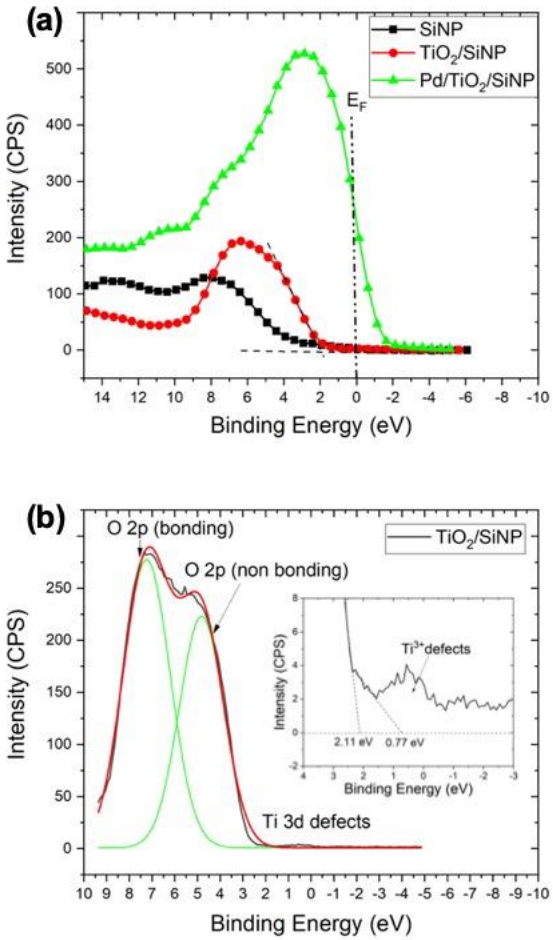


**Figure 7**. (a) Valence band spectra plotted for all the samples; (b) deconvoluted valence band spectra of the $TiO_2$/SiNP sample; (inset) magnified details.

The VB spectrum for the SiNP sample is in a good agreement with those reported for porous Si [28]. The VB maximum (VBM) was estimated using standard method as described elsewhere [22,29]. The VBM of Pd was observed at approximately 2.1 eV above the Fermi level ($E_F$) indicating the metallic behavior of the top palladium layer [23], while the VBM of the $TiO_2$/SiNP sample showed a value 2.11 eV below the $E_F$.

The VB peak for the of the $TiO_2$/SiNP sample was deconvoluted into two components located at 4.5 eV and 7 eV and corresponding to the O 2p non-bonding orbitals and O 2p – Ti 3d hybridized states, respectively (Figure 7b) [22,30]. It is also visible a small peak located at 0.6eV with respect to the Fermi level, and the defect edge with a VBM at 0.77 eV. These VB features correspond to the Ti 3d defects states, which are mostly attributed to oxygen vacancies ($V_o$) as reported by Laidani *et al.*[31] and Luciu *et al.*[32], and/or to $Ti^{3+}$ defects on the surface [33]. These defects are considered to play a crucial role in photocatalytic processes [34]. They improve the absorbance narrowing the band gap, increase the mobility of photogenerated charge carriers and enhance the photoelectrochemical/photocatalytic activity. As shown in this study, the Pd coating decreases the concentration of photoactive defects, and as a consequence, it reduces the PEC efficiency of $TiO_2$. On the other hands, the Pd coating boosts the electrocatalytic efficiency. Therefore, some balance between photo- and electro- catalytic behaviors should be established in order to effectively apply Pd/$TiO_2$/SiNP nanocomposites for the catalytic performance.

## 4. Conclusions

In this work, we have studied the structural, chemical and electronic properties of Pd coated $TiO_2$/Si nanopillars fabricated by ALD and MACE by means of electron microscopy, ToF-SIMS, AES and X-ray photoelectron spectroscopy. The chemical composition and morphology of nanocomposites were established. It was determined that ALD metallic layer consisting of Pd nanoparticles coats the $TiO_2$/Si nanopillars conformally. The ToF-SIMS mapping demonstrated the inhomogeneous distribution of metal elements because of hydrocarbon contaminations over the surface. The inhomogeneous distribution of Pd may cause a non-uniformity of the electrical potential over the surface, and as a consequence, it can modify the (photo)catalytic activity of the produced nanocomposites. It was shown that after the ALD Pd deposition, the phase composition of the $TiO_2$ layer improves that can be explained by the decrease of defects concentration.

**Acknowledgements**

Authors acknowledge the support of RISE- H2020-EU.1.3.3. grant (ID:778157) CanBioSe. **I.I.** also acknowledges the financial support from the NCN of Poland by the SONATA 11 project UMO-2016/21/D/ST3/00962

**Author Contributions:**

All authors have given approval to the final version of the manuscript.

**References**

[1] Y. He, C. Jiang, H. Yin, W. Yuan, Tailoring the wettability of patterned silicon surfaces with dual-scale pillars: From hydrophilicity to superhydrophobicity, Appl. Surf. Sci. 257 (2011) 7689–7692. doi:10.1016/j.apsusc.2011.04.009.

[2] B.D. Choudhury, R. Casquel, M.J. Bañuls, F.J. Sanza, M.F. Laguna, M. Holgado, R. Puchades, A. Maquieira, C.A. Barrios, S. Anand, Silicon nanopillar arrays with SiO2 overlayer for biosensing application, Opt. Mater. Express. 4 (2014) 1345. doi:10.1364/OME.4.001345.

[3] V. Myndrul, E. Coy, M. Bechelany, I. Iatsunskyi, Photoluminescence label-free immunosensor for the detection of Aflatoxin B1 using polyacrylonitrile/zinc oxide nanofibers, Mater. Sci. Eng. C. 118 (2021) 111401. doi:https://doi.org/10.1016/j.msec.2020.111401.

[4] F.-Q. Zhang, Y. Hu, R.-N. Sun, H. Fu, K.-Q. Peng, Gold-Sensitized Silicon/ZnO Core/Shell Nanowire Array for Solar Water Splitting, Front. Chem. 7 (2019) 206. doi:10.3389/fchem.2019.00206.

[5] M. Pavlenko, K. Siuzdak, E. Coy, M. Jancelewicz, S. Jurga, I. Iatsunskyi, Silicon/TiO2 core-shell nanopillar photoanodes for enhanced photoelectrochemical water oxidation, Int. J. Hydrogen Energy. 42 (2017) 30076–30085. doi:10.1016/j.ijhydene.2017.10.033.

[6] M. Pavlenko, K. Siuzdak, E. Coy, K. Załęski, M. Jancelewicz, I. Iatsunskyi, Enhanced solar-driven water splitting of 1D core- shell Si/TiO 2 /ZnO nanopillars, Int. J. Hydrogen Energy. 45 (2020) 26426–26433. doi:10.1016/j.ijhydene.2019.11.231.

[7] M. Pavlenko, E.L. Coy, M. Jancelewicz, K. Załęski, V. Smyntyna, S. Jurga, I. Iatsunskyi, K. Zaleski, V. Smyntyna, S. Jurga, I. Iatsunskyi, Enhancement of optical and mechanical properties of Si nanopillars by ALD TiO2 coating, RSC Adv. 6 (2016) 97070–97076. doi:10.1039/C6RA21742G.

[8] A. Kertmen, E. Barbé, M. Szkoda, K. Siuzdak, V. Babačić, P. Torruella, I. Iatsunskyi, M. Kotkowiak, K. Rytel, S. Estradé, F. Peiró, S. Jurga, Y. Li, E. Coy, Photoelectrochemically Active N-Adsorbing Ultrathin TiO 2 Layers for Water-Splitting Applications Prepared by

Pyrolysis of Oleic Acid on Iron Oxide Nanoparticle Surfaces under Nitrogen Environment, Adv. Mater. Interfaces. (2018) 1801286. doi:10.1002/admi.201801286.

[9] O. Graniel, V. Fedorenko, R. Viter, I. Iatsunskyi, G. Nowaczyk, M. Weber, K. Załęski, S. Jurga, V. Smyntyna, P. Miele, A. Ramanavicius, S. Balme, M. Bechelany, Optical properties of ZnO deposited by atomic layer deposition (ALD) on Si nanowires, Mater. Sci. Eng. B. 236–237 (2018) 139–146. doi:10.1016/j.mseb.2018.11.007.

[10] L. Cheng, D. Zhang, Y. Liao, F. Li, H. Zhang, Q. Xiang, Constructing functionalized plasmonic gold/titanium dioxide nanosheets with small gold nanoparticles for efficient photocatalytic hydrogen evolution, J. Colloid Interface Sci. 555 (2019) 94–103. doi:https://doi.org/10.1016/j.jcis.2019.07.060.

[11] A. Barhoum, H.H. El-Maghrabi, I. Iatsunskyi, E. Coy, A. Renard, C. Salameh, M. Weber, S. Sayegh, A.A. Nada, S. Roualdes, M. Bechelany, Atomic layer deposition of Pd nanoparticles on self-supported carbon-Ni/NiO-Pd nanofiber electrodes for electrochemical hydrogen and oxygen evolution reactions, J. Colloid Interface Sci. 569 (2020) 286–297. doi:https://doi.org/10.1016/j.jcis.2020.02.063.

[12] E. Coy, K. Siuzdak, M. Pavlenko, K. Załęski, O. Graniel, M. Ziółek, S. Balme, P. Miele, M. Weber, M. Bechelany, I. Iatsunskyi, Enhancing photocatalytic performance and solar absorption by schottky nanodiodes heterojunctions in mechanically resilient palladium coated TiO2/Si nanopillars by atomic layer deposition, Chem. Eng. J. 392 (2020) 123702. doi:https://doi.org/10.1016/j.cej.2019.123702.

[13] Y.E. Silina, M. Koch, P. Herbeck-Engel, I. Iatsunskyi, Exploring the potential of high resolution inductively coupled plasma mass spectrometry towards non-destructive control and validation of electroless gold nanoparticles onto silicon nanowires hybrids, Anal. Methods. 11 (2019) 3987–3995. doi:10.1039/C9AY01182J.

[14] A.G. Shard, X-ray photoelectron spectroscopy, in: Charact. Nanoparticles, Elsevier, 2020: pp. 349–371. doi:10.1016/B978-0-12-814182-3.00019-5.

[15] I. Iatsunskyi, M. Kempiński, M. Jancelewicz, K. Załęski, S. Jurga, V. Smyntyna, Structural and XPS characterization of ALD Al2O3 coated porous silicon, Vacuum. 113 (2015) 52–58. doi:10.1016/j.vacuum.2014.12.015.

[16] I. Brytavskyi, K. Hušeková, V. Myndrul, M. Pavlenko, E. Coy, K. Zaleski, D. Gregušová, L. Yate, V. Smyntyna, I. Iatsunskyi, Effect of porous silicon substrate on structural, mechanical and optical properties of MOCVD and ALD ruthenium oxide nanolayers, Appl. Surf. Sci. 471 (2019) 686–693. doi:10.1016/j.apsusc.2018.12.022.

[17] I. Iatsunskyi, A. Vasylenko, R. Viter, M. Kempiński, G. Nowaczyk, S. Jurga, M. Bechelany, Tailoring of the electronic properties of ZnO-polyacrylonitrile nanofibers:

Experiment and theory, Appl. Surf. Sci. 411 (2017) 494–501. doi:10.1016/j.apsusc.2017.03.111.

[18] J. Światowska-Mrowiecka, F. Martin, V. Maurice, S. Zanna, L. Klein, J. Castle, P. Marcus, The distribution of lithium intercalated in V2O5 thin films studied by XPS and ToF-SIMS, Electrochim. Acta. 53 (2008) 4257–4266. doi:10.1016/j.electacta.2007.12.083.

[19] E.Y. Silina, V.K. Gernaey, D. Semenova, I. Iatsunskyi, Application of Organic-Inorganic Hybrids in Chemical Analysis, Bio- and Environmental Monitoring, Appl. Sci. . 10 (2020). doi:10.3390/app10041458.

[20] H. Feng, J.W. Elam, J.A. Libera, W. Setthapun, P.C. Stair, Palladium Catalysts Synthesized by Atomic Layer Deposition for Methanol Decomposition, Chem. Mater. 22 (2010) 3133–3142. doi:10.1021/cm100061n.

[21] G. Speranza, R. Canteri, RxpsG a new open project for Photoelectron and Electron Spectroscopy data processing, SoftwareX. 10 (2019) 100282. doi:10.1016/j.softx.2019.100282.

[22] I. Iatsunskyi, M. Kempiński, G. Nowaczyk, M. Jancelewicz, M. Pavlenko, K. Załęski, S. Jurga, Structural and XPS studies of PSi/TiO2 nanocomposites prepared by ALD and Ag-assisted chemical etching, Appl. Surf. Sci. 347 (2015) 777–783. doi:10.1016/j.apsusc.2015.04.172.

[23] M. Brun, A. Berthet, J.. Bertolini, XPS, AES and Auger parameter of Pd and PdO, J. Electron Spectros. Relat. Phenomena. 104 (1999) 55–60. doi:10.1016/S0368-2048(98)00312-0.

[24] A. Lion, N. Laidani, P. Bettotti, C. Piotto, G. Pepponi, M. Barozzi, M. Scarpa, Angle resolved XPS for selective characterization of internal and external surface of porous silicon, Appl. Surf. Sci. 406 (2017) 144–149. doi:10.1016/j.apsusc.2017.02.099.

[25] I. Iatsunskyi, M. Jancelewicz, G. Nowaczyk, M. Kempiński, B. Peplińska, M. Jarek, K. Załęski, S. Jurga, V. Smyntyna, Atomic layer deposition TiO2 coated porous silicon surface: Structural characterization and morphological features, Thin Solid Films. 589 (2015) 303–308. doi:10.1016/j.tsf.2015.05.056.

[26] J. Schneider, M. Matsuoka, M. Takeuchi, J. Zhang, Y. Horiuchi, M. Anpo, D.W. Bahnemann, Understanding TiO $_2$ Photocatalysis: Mechanisms and Materials, Chem. Rev. 114 (2014) 9919–9986. doi:10.1021/cr5001892.

[27] T.L. Thompson, J.T. Yates, TiO2-based Photocatalysis: Surface Defects, Oxygen and Charge Transfer, Top. Catal. 35 (2005) 197–210. doi:10.1007/s11244-005-3825-1.

[28] R.R. Kunz, P.M. Nitishin, H.R. Clark, M. Rothschild, B. Ahern, Observation of a

nanocrystalline-to-amorphous phase transition in luminescent porous silicon, Appl. Phys. Lett. 67 (1995) 1766–1768. doi:10.1063/1.114376.

[29] M.M. Khan, S.A. Ansari, D. Pradhan, M.O. Ansari, D.H. Han, J. Lee, M.H. Cho, Band gap engineered TiO 2 nanoparticles for visible light induced photoelectrochemical and photocatalytic studies, J. Mater. Chem. A. 2 (2014) 637–644. doi:10.1039/C3TA14052K.

[30] U. Diebold, The surface science of titanium dioxide, Surf. Sci. Rep. 48 (2003) 53–229. doi:10.1016/S0167-5729(02)00100-0.

[31] N. Laidani, P. Cheyssac, J. Perrière, R. Bartali, G. Gottardi, I. Luciu, V. Micheli, Intrinsic defects and their influence on the chemical and optical properties of TiO 2− x films, J. Phys. D. Appl. Phys. 43 (2010) 485402. doi:10.1088/0022-3727/43/48/485402.

[32] I. Luciu, R. Bartali, N. Laidani, Influence of hydrogen addition to an Ar plasma on the structural properties of TiO 2− x thin films deposited by RF sputtering, J. Phys. D. Appl. Phys. 45 (2012) 345302. doi:10.1088/0022-3727/45/34/345302.

[33] K. Bapna, D.M. Phase, R.J. Choudhary, Study of valence band structure of Fe doped anatase TiO2 thin films, J. Appl. Phys. 110 (2011) 2–8. doi:10.1063/1.3624775.

[34] A. Sirisuk, E. Klansorn, P. Praserthdam, Effects of reaction medium and crystallite size on Ti3+ surface defects in titanium dioxide nanoparticles prepared by solvothermal method, Catal. Commun. 9 (2008) 1810–1814. doi:10.1016/j.catcom.2008.01.035.